Supplemental Materials: Binary-coupling sparse SYK model

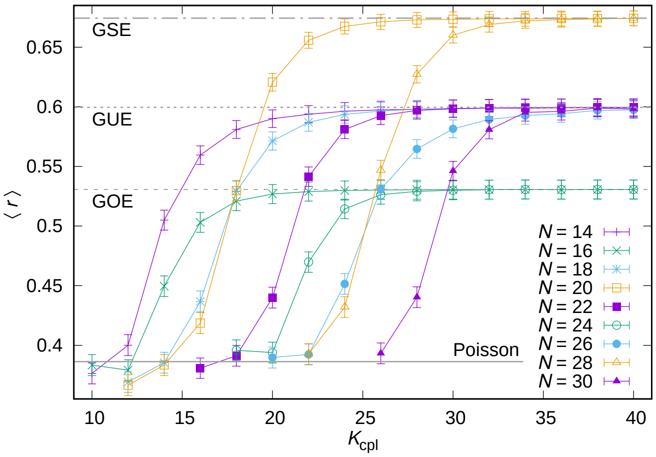

FIG. S1. The average of neighboring gap ratio between non-degenerate eigenvalues for unary sparse samples with least degeneracy, plotted against the number of nonzero couplings. "GSE", "GUE", "GOE", and "Poisson" indicate the values in Ref. [46].

S1. UNARY-COUPLING SPARSE SYK MODEL

As we have stated in Sec. II of the main text, the unary-coupling sparse SYK model (i.e., all nonzero couplings are $+1$) behaves similarly to the binary-coupling model as long as $1 \ll K_{\mathrm{cpl}} \ll N_{\mathrm{total}}$. Below, we will show basic results regarding the unary-coupling model.

In the binary-coupling sparse SYK model, there were two sources of randomness: (i) which coupling is nonzero, and (ii) whether each nonzero coupling is $+1$ or -1. In the unary-coupling model, the only source of randomness is (i). Therefore, if K_{cpl} is too small or too large, it is far less effective than the binary-coupling model. Specifically, when $K_{\mathrm{cpl}} = N_{\mathrm{total}}$, there is no randomness at all.

The anti-commuting relation between Majorana fermions (2) means that reordering the Majorana fermions $(\chi_1, \chi_2, \ldots, \chi_N) \mapsto \left(\chi_{\sigma(1)}, \chi_{\sigma(2)}, \ldots, \chi_{\sigma(N)}\right)$, where σ is a non-unit element of the symmetry group S_N, can flip some of the signs of the interaction. For $1 \ll K_{\mathrm{cpl}} \ll N_{\mathrm{total}}$, for a typical choice of the nonzero terms, it would be possible to perform the reordering to the binary-coupling model and make most of the signs to be positive, then we do not expect a big difference between ensembles of the binary-coupling and unary-coupling model realizations.

In Fig. S1, we plot the average of neighboring gap ratio between non-degenerate eigenvalues for the *unary*-coupling sparse SYK model. The observed values are nearly identical to those for the *binary*-coupling model in Fig. 2 in the main text. In Fig. S2, we plot the spectral form factor for the unary-coupling model. Again, the results exhibit little difference from the binary-coupling model in Fig. 3 in the main text. Note that changing all nonzero J_{abcd} for a particular realization of the binary-coupling model results in a significant change of its spectrum. The observed agreement between the two models is between their ensembles after the averaging.

S2. EXAMPLE OF SINGLE REALIZATIONS FOR $N = 32, 34$

In Fig. S3, we show the distributions for the unfolded nearest-neighbor level separation $P(s)$ and neighboring gap ratio $P(r)$ for single realizations of the binary-coupling sparse SYK model for $(N, K_{\mathrm{cpl}}) = (32, 30), (34, 36)$. The Hamiltonian we used are

$$\begin{aligned}\mathcal{H} = {} & \chi_1\chi_2\chi_3\chi_4 - \chi_1\chi_6\chi_{10}\chi_{21} - \chi_1\chi_8\chi_{23}\chi_{24} \\ & - \chi_1\chi_{11}\chi_{27}\chi_{28} + \chi_1\chi_{22}\chi_{26}\chi_{27} + \chi_2\chi_5\chi_{10}\chi_{23} \\ & + \chi_2\chi_{15}\chi_{25}\chi_{30} + \chi_3\chi_5\chi_{10}\chi_{32} - \chi_3\chi_5\chi_{24}\chi_{31} \\ & + \chi_3\chi_{20}\chi_{24}\chi_{26} + \chi_4\chi_8\chi_{18}\chi_{23} - \chi_5\chi_{10}\chi_{23}\chi_{30} \\ & + \chi_5\chi_{19}\chi_{23}\chi_{30} - \chi_5\chi_{25}\chi_{29}\chi_{32} - \chi_6\chi_7\chi_{20}\chi_{23} \\ & + \chi_7\chi_9\chi_{12}\chi_{15} + \chi_7\chi_{10}\chi_{12}\chi_{18} - \chi_7\chi_{21}\chi_{23}\chi_{27} \\ & - \chi_7\chi_{24}\chi_{28}\chi_{31} + \chi_8\chi_9\chi_{15}\chi_{32} - \chi_9\chi_{15}\chi_{25}\chi_{30} \\ & + \chi_9\chi_{19}\chi_{21}\chi_{27} + \chi_{10}\chi_{11}\chi_{19}\chi_{32} + \chi_{10}\chi_{12}\chi_{14}\chi_{16} \\ & - \chi_{11}\chi_{17}\chi_{25}\chi_{28} - \chi_{12}\chi_{14}\chi_{20}\chi_{24} - \chi_{12}\chi_{19}\chi_{31}\chi_{32} \\ & + \chi_{12}\chi_{23}\chi_{24}\chi_{30} - \chi_{13}\chi_{17}\chi_{21}\chi_{27} - \chi_{22}\chi_{23}\chi_{26}\chi_{31},\end{aligned} \tag{S1}$$

for $N = 32$ and

$$\begin{aligned}\mathcal{H} = {} & \chi_1\chi_6\chi_{20}\chi_{28} + \chi_1\chi_7\chi_{22}\chi_{24} - \chi_1\chi_{10}\chi_{15}\chi_{25} \\ & - \chi_1\chi_{15}\chi_{19}\chi_{31} - \chi_1\chi_{15}\chi_{21}\chi_{26} - \chi_2\chi_3\chi_{17}\chi_{23} \\ & + \chi_2\chi_{19}\chi_{23}\chi_{24} + \chi_3\chi_5\chi_6\chi_{16} + \chi_3\chi_{14}\chi_{17}\chi_{22} \\ & + \chi_3\chi_{15}\chi_{20}\chi_{25} + \chi_3\chi_{21}\chi_{28}\chi_{34} + \chi_3\chi_{23}\chi_{32}\chi_{33} \\ & + \chi_4\chi_5\chi_6\chi_{30} - \chi_4\chi_9\chi_{15}\chi_{29} - \chi_4\chi_9\chi_{30}\chi_{32} \\ & + \chi_4\chi_{22}\chi_{27}\chi_{30} - \chi_4\chi_{23}\chi_{26}\chi_{34} + \chi_5\chi_8\chi_{14}\chi_{31} \\ & - \chi_5\chi_{10}\chi_{15}\chi_{18} - \chi_6\chi_7\chi_{18}\chi_{30} + \chi_6\chi_{13}\chi_{30}\chi_{32} \\ & - \chi_6\chi_{14}\chi_{20}\chi_{25} - \chi_6\chi_{15}\chi_{23}\chi_{32} - \chi_6\chi_{18}\chi_{32}\chi_{34} \\ & + \chi_6\chi_{21}\chi_{31}\chi_{32} - \chi_7\chi_{24}\chi_{28}\chi_{30} + \chi_8\chi_{13}\chi_{14}\chi_{19} \\ & + \chi_9\chi_{11}\chi_{25}\chi_{29} - \chi_{10}\chi_{13}\chi_{21}\chi_{34} + \chi_{11}\chi_{12}\chi_{29}\chi_{33} \\ & + \chi_{11}\chi_{22}\chi_{28}\chi_{30} - \chi_{13}\chi_{21}\chi_{23}\chi_{25} + \chi_{15}\chi_{18}\chi_{27}\chi_{28} \\ & - \chi_{16}\chi_{25}\chi_{27}\chi_{28} - \chi_{17}\chi_{19}\chi_{24}\chi_{28} - \chi_{19}\chi_{25}\chi_{31}\chi_{33},\end{aligned} \tag{S2}$$

for $N = 34$. The results agree well with those for the GOE and GUE random matrices [46, 56], respectively.

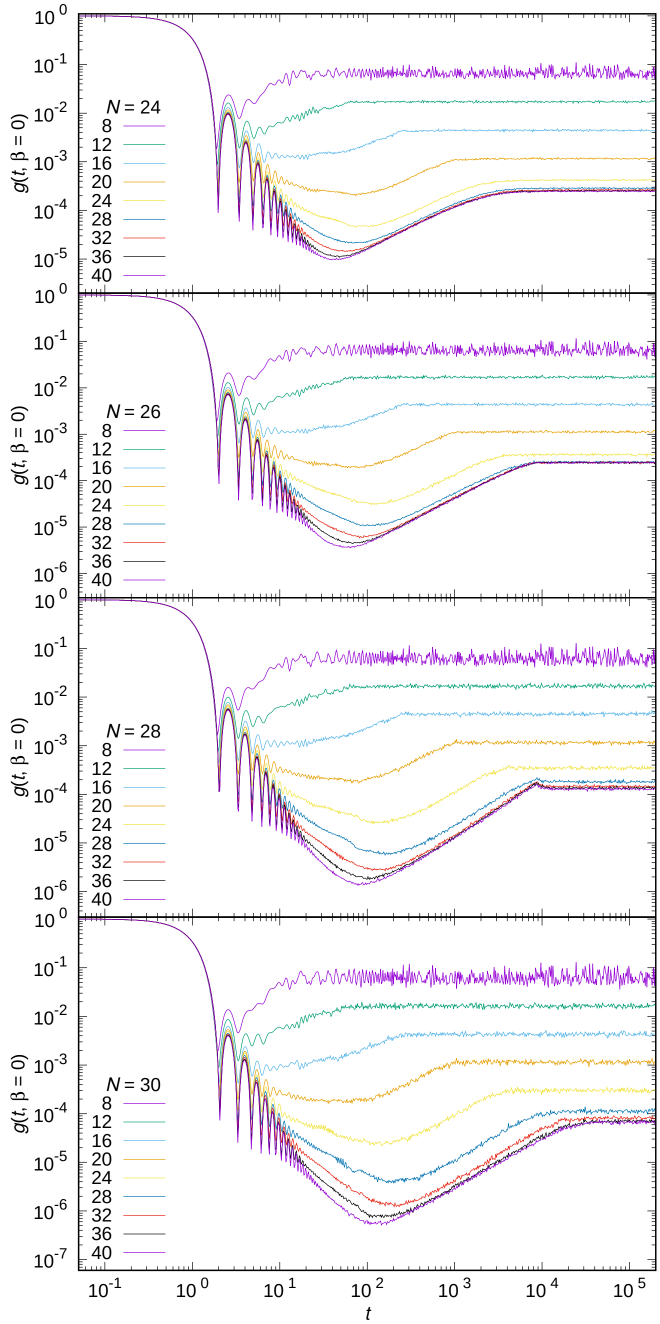

FIG. S2. The spectral form factor $g(t, \beta = 0)$ versus time t for the unary-coupling sparse SYK model. The value of N as well as the number of nonzero couplings, $K_{\rm cpl}$, are indicated in the legend for each plot.

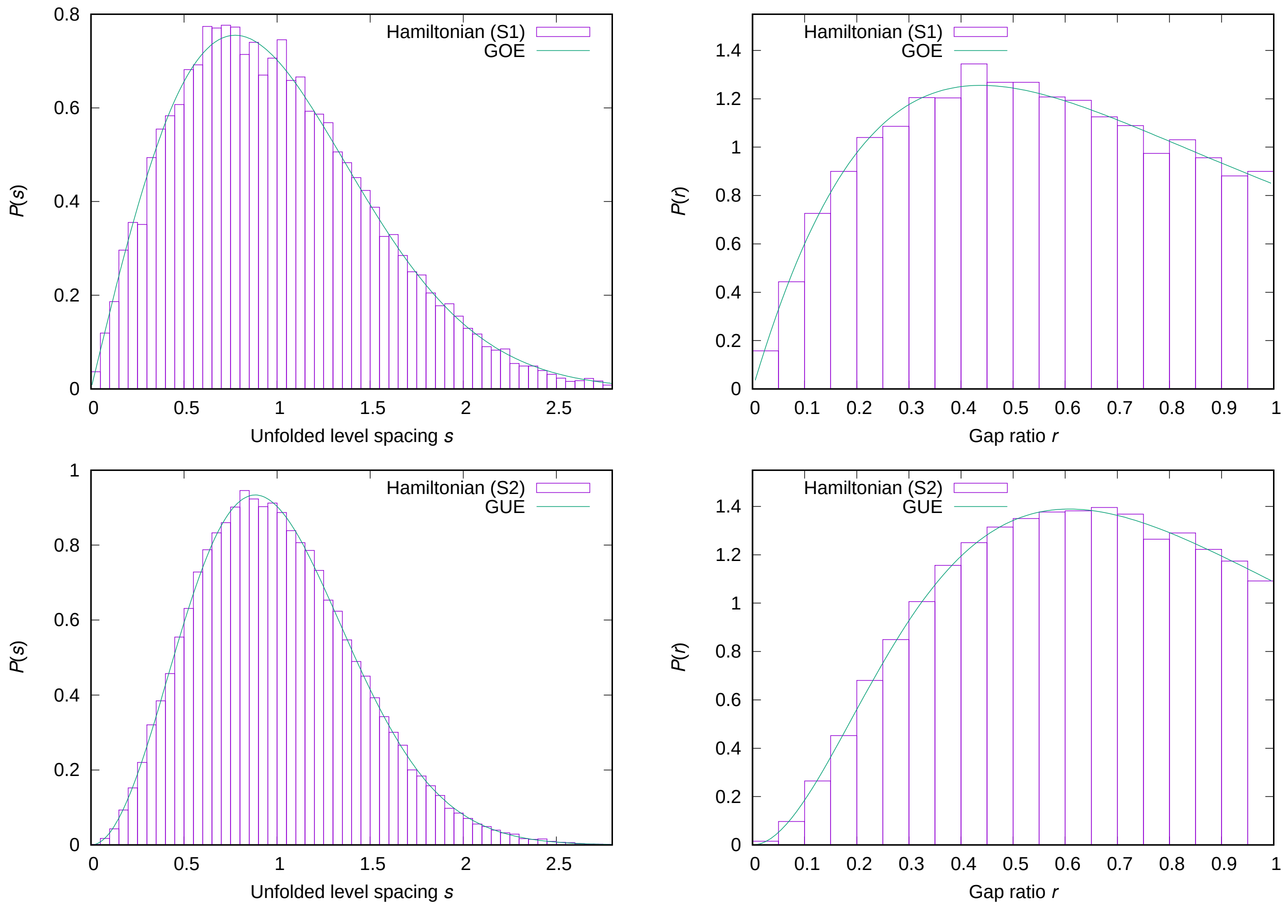

FIG. S3. The distribution of the nearest-neighbor level spacing $P(s)$ and that of the neighboring gap ratio $P(r)$ for the eigenvalues of the single realization of the binary sparse SYK model. [Top] $N = 32$ and $K_{\mathrm{cpl}} = 30$ with the specific realization given by eq. (S1), [Bottom] $N = 34$ and $K_{\mathrm{cpl}} = 36$ with the specific realization given by eq. (S2). For $P(s)$, we omit the largest 5% and smallest 5% of the eigenvalues from the analysis to prevent the eigenvalues near the edges from affecting the polynomial fit of the spectrum. We use tenth-order polynomial fitting for unfolding the spectrum.